**Rare Metal Materials and Engineering**
Volume 54, Issue 8, August 2025
Available online at www.rmme.ac.cn

Science Press

**Cite this article as**: Yang Yajie, Xu Liujie, Fang Hong, et al. Effect of Zirconia Content on Microstructure and Abrasive Wear Properties of TZM Alloy[J]. Rare Metal Materials and Engineering, 2025, 54(08): 1962-1970. DOI: https://doi.org/10.12442/j.issn.1002-185X.20240384.

ARTICLE

# Effect of Zirconia Content on Microstructure and Abrasive Wear Properties of TZM Alloy

**Yang Yajie[1], Xu Liujie[1,2], Fang Hong[3], Li Zhou[2], Li Xiuqing[2], Wei Shizhong[2]**

*[1] School of Materials Science and Engineering, Henan University of Science and Technology, Luoyang 471000, China; [2] National Joint Engineering Research Center for Abrasion Control and Molding of Metal Materials, Henan University of Science and Technology, Luoyang 471003, China; [3] Fonlink Photoelectric (LuoYang) Co., Ltd, Luoyang 471000, China*

**Abstract:** The TZM alloys with different contents of $ZrO_2$ were prepared by powder metallurgy and rolling, and the grain size, hardness, and abrasive wear resistance of TZM alloy were studied. The abrasive wear test of TZM alloy was conducted under the conditions of 10, 15, and 20 N and abrasive particle sizes of 7, 11, 18, and 38 μm. The results show that the added $ZrO_2$ particles in TZM alloy are mainly distributed at the grain boundaries. The grains of TZM alloy containing 1.5wt% $ZrO_2$ are significantly refined, and the hardness is increased by 16%. The wear test results show that TZM alloy containing 1.5wt% $ZrO_2$ has the lowest mass loss rate and excellent wear resistance under all loads and abrasive sizes, and the wear performance is improved by 12%. The $ZrO_2$ with high hardness becomes the main bearer of the load, and as the second-phase, it hinders the abrasive particles from entering the matrix and effectively resists the scratch of the abrasive particles, which is the main reason for the excellent wear resistance.

**Key words:** TZM alloy; zirconium oxide; abrasive wear; grain size

## 1 Introduction

Molybdenum has good high-temperature strength and high-temperature hardness, excellent wear resistance and corrosion resistance, and is widely used in aerospace, defense, military industry, mechanical processing, nuclear energy, and electronics[1–6]. However, due to its brittleness, low recrystallization temperature, and low room-temperature strength, its wide application as a structural material is restricted. Alloying is one of the main methods to improve its performance. Common molybdenum alloys include MHC, TZM, TZC, etc[6–10]. The widely used TZM alloy is a pure molybdenum-based alloy containing 0.5wt% – 0.8wt% Ti, 0.08wt% – 0.10wt% Zr, and 0.01wt%–0.04wt% C[5]. In TZM alloy, Ti, Zr, and C are used as alloying elements to enhance the properties of the alloy by solid solution strengthening and second-phase strengthening mechanisms. Ti and Zr are added to TZM alloy to prevent grain growth by forming TiC and ZrC at grain boundaries, thereby contributing to excellent strength. Due to the formation of these carbides, the hardness of TZM alloy at different sintering temperatures is higher than that of pure Mo.

TZM has excellent strength and creep resistance at temperatures up to 1200 °C. It is used in the manufacture of molds and punches to effectively eliminate the deformation (wear) of mold materials during sintering and removal of ceramic materials from molds[11]. However, TZM alloy is difficult to resist severe abrasive wear during use, so the service life of mold and punch is not ideal. Therefore, how to further improve the wear resistance of TZM alloy is of great significance in the field of modern manufacturing. Studies have shown that the addition of TiC[12], ZrC[4], $La_2O_3$[13], $Al_2O_3$[14], $ZrO_2$[15], and other second-phase particles in molybdenum alloy can effectively refine the grain size, hinder dislocation movement, and improve the hardness and strength of the alloy. Zhou et al[16] studied the wear resistance of TZM alloy by adding $Al_2O_3$, and pointed out that due to the high hardness and self-lubrication effect of $Al_2O_3$, the movement of dislocations at grain boundaries was prevented by refining Mo matrix grains, and the hardness and strength of the alloy were improved. Sirali et al[17–18] found that the wear resistance of

Received date: July 27, 2024
Foundation item: National Natural Science Foundation of China (U1804124); Key Scientific and Technological Project of Henan Province (202102210014)
Corresponding author: Xu Liujie, Ph. D., Professor, National Joint Engineering Research Center for Abrasion Control and Molding of Metal Materials, Henan University of Science and Technology, Luoyang 471003, P. R. China, E-mail: xlj@haust.edu.cn

TZM alloys with different amounts of elements Ti and Zr was improved, and with the increase in Ti and Zr content, the grain size decreased while the hardness increased. Tuzemen et al[4] produced TZM-TiC and TZM-ZrC composites by spark plasma sintering. The addition of carbides can refine grains and improve the hardness of materials. The hardness of TZM-TiC composite is higher than that of TZM-ZrC composite, up to 4.1 GPa. The grain size of Mo alloy can be reduced by adding submicron levels of second-phase $ZrO_2$. The grain size of the Mo-0.4%$ZrO_2$ alloy sheet prepared by Xu et al[19] was refined from 11.3 μm of pure Mo to 5.8 μm, which is due to a large amount of $ZrO_2$ distributed at the grain boundaries. In addition, the addition of $ZrO_2$ changes the slip system of Mo alloy from [110] to [123], increasing the number of slip systems. Therefore, the elongation of Mo alloy is increased. Cui et al[20] studied the properties of Mo-$ZrO_2$ alloy prepared by hydrothermal method, and the tensile strength and yield strength were increased by 32.33% and 53.76%, respectively, compared with those of pure Mo. $ZrO_2$ has higher hardness, higher melting point, and better chemical stability than other second-phases, so it is selected as a second-phase particle to enhance the molybdenum alloy matrix. In this study, TZM alloy was produced by powder metallurgy method. The effect of adding three contents of $ZrO_2$ in TZM alloy on grain size, and the effect of grain size change on the microstructure, hardness, and abrasive wear properties of the alloy were studied.

## 2 Experiment

TZM alloy matrix powders used in this study include Mo powder (average particle size $d$=2–3 μm, purity of 99%), $TiH_2$ powder (average particle size $d$=5 – 10 μm, purity of 99%), $ZrH_2$ powder (average particle size $d$=2 – 10 μm, purity of 99%), and C powder (average particle size $d$=15 – 30 μm, purity of 99%). $ZrO_2$ powder (average particle size $d$=50 nm, purity of 99%) was obtained from Hangzhou Zhitai Purification Technology Co., Ltd. To meet the needs for large-scale industrial production, the powders were mixed by solid-solid mixing method according to the proportion of components in Table 1. The sintered samples were rolled by cold isostatic pressing machine (LD1710/2000-300YS) at 180 MPa for 30 min and medium frequency induction sintering furnace (GH800×1200) at the highest sintering temperature of 2000 °C, and the total sintering time was 60 h.

The Vickers hardness of the sample was measured by MH-3 microhardness tester. To reduce the experimental error, the upper and lower surfaces of the polished sample were parallel and smooth before measurement, and the average of five data was taken. In the experiment, the actual density of TZM alloy was measured by ME203E/02 density tester, the density of three samples in each group was measured by Archimedes drainage method, and the average value was calculated.

**Table 1 Chemical composition of TZM alloys (wt%)**

| Alloy No. | Ti | Zr | C | $ZrO_2$ | Mo |
|---|---|---|---|---|---|
| 1 | 0.5 | 0.1 | 0.03 | 0 | 99.37 |
| 2 | 0.5 | 0.1 | 0.03 | 0.5 | 98.87 |
| 3 | 0.5 | 0.1 | 0.03 | 1.0 | 98.37 |
| 4 | 0.5 | 0.1 | 0.03 | 1.5 | 97.87 |

ML-100 pin disc wear testing machine was used to test the wear performance of the sample. The size of TZM alloy tested was 4.5 mm×4.5 mm and the thickness was 1 mm. The schematic diagram of the working principle of the testing machine is shown in Fig. 1. The rotation speed of the test machine disc was 60 r/min. The $Al_2O_3$ sandpapers with different particle sizes were fixed on the disk, and the average particle sizes were 7, 11, 18, and 38 μm, separately. Under the load of 10, 15, and 20 N, the sample moved from the center of the disc to the edge at a speed of 6 mm/s, and each sample moved back and forth for 10 times. Before the test, each sample was polished to the same roughness using sandpaper with a mesh of 800, 1200, 1500, and 2000 to make the surface as smooth as possible. The mass of the samples before and after wear was measured by TG328B analytical balance with relative accuracy of 0.1 mg. For the accuracy of the experiment, the wear results were determined by the mean values of three sets of parallel tests.

The phase composition and type of TZM alloy were identified by X-ray diffractometer (XRD, D8 Advance Bruker, Germany) with Cu-Kα_1 radiation. The microstructure of TZM alloy before and after wear was observed by scanning electron microscope (SEM, VEGA3-TESCAN-SBH). The components of the second-phase as well as the elemental content and distribution on the wear surface were analyzed using energy dispersive spectrometer (EDS). Before the test, the samples were mechanically polished, and the impurities were removed by ultrasonic vibration with alcohol for 5 min before the wear test. The grain size was measured by selecting 20 fields of view in the SEM image at 1000 times for each sample. Image J (Image processing software) was used to perform 200 measurements and statistics, and the result was determined as the particle size distribution.

## 3 Results and Discussion

### 3.1 Microstructure

The SEM images of the microstructure of TZM alloy with

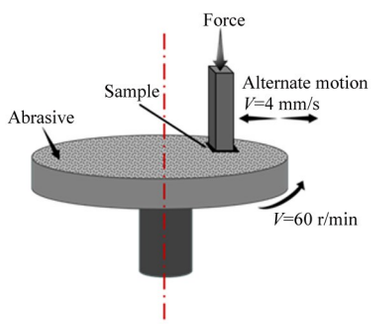


Fig.1 Schematic diagram of working principle of ML-100 abrasive wear tester

different contents of $ZrO_2$ are given in Fig.2. It can be clearly seen that with the increase in content of $ZrO_2$, the larger black second-phase particles in the alloy gradually become smaller and smaller, which are uniformly dispersed with $ZrO_2$ in the TZM alloy matrix, and the black second-phase particles change from being located at two or three grain boundaries to being squeezed by more grain boundaries, thus becoming smaller in size. To confirm the chemical composition of the black area in the alloy matrix, the pure TZM alloy was scanned by EDS, and the element mapping is shown in Fig.3. The second-phase particles in the figure have also been reported in other literatures, one is an oxide rich in Ti-O, and the other is an oxide rich in Ti-Zr-O, because the element Ti in TZM alloy tends to combine with element O to form compounds[21]. Because the decomposition temperature of $TiH_2$ is lower than that of $ZrH_2$ during the sintering, the decomposed [Ti] will react with oxygen to form $TiO_2$ first[22]. Based on thermodynamic analysis, the Gibbs free energy change ($\Delta G$) of the reaction of $TiH_2$ and $ZrH_2$ with C is larger than that with O. Therefore, the oxidation process of $TiH_2$ and $ZrH_2$ is preferable than the reduction process[23]. Furthermore, during the sintering process, the elements O and C in the TZM alloy are present in the Mo matrix in the form of a solid solution. The electronegativity of elements Ti and Zr is greater than that of the Mo element, which results in a greater tendency for these elements to form oxides.

As the temperature rises, the active elements Ti and Zr decompose from $TiH_2$ and $ZrH_2$, respectively. This results in the reduction of O dissolved in Mo by a substitution reaction, which precipitates the O atoms from the Mo matrix, thereby forming a stable second-phase oxide. Besides the titanium and zirconium oxides, $ZrTiO_4$ has the lowest $\Delta G$ value and thus is easier to form. At temperatures above 1200 ° C, titanium and zirconium react with O to form $ZrTiO_4$ ($Ti+Zr+2O_2=ZrTiO_4$)[24]. The black irregular-shaped second-phase particles is ascertained to be $TiO_2$ or $ZrTiO_4$. Fig.4 shows that the grain size decreases significantly with the increase in $ZrO_2$ content. The average grain sizes are 31.47, 16.43, 16.10, and 9.81 μm. When 0.5wt% $ZrO_2$ is added to the TZM alloy, the grain size is mainly distributed within 5–20 μm, accounting for about 77%. In the same grain size range, the total grain size distribution is almost the same as that when 1.0wt% $ZrO_2$ is added, but it is worth mentioning that compared with the case when 0.5wt% $ZrO_2$ is added, the proportion of grain size within 10–15 μm is more. The grain refinement of TZM alloy with 1.5wt% $ZrO_2$ addition is the most obvious, almost all below 14 μm. The addition of $ZrO_2$ refines the grains of the alloy, because grain growth is a process of grain boundary displacement. As the second-phase, $ZrO_2$ is evenly distributed in TZM alloy to pin grain boundaries and to hinder grain boundary migration, which reduces the growth rate of grains, and the particles distributed at grain boundaries have a pinning effect on grain boundary expansion[25]. The grain size of the matrix is related to the doped second-phase particles. If

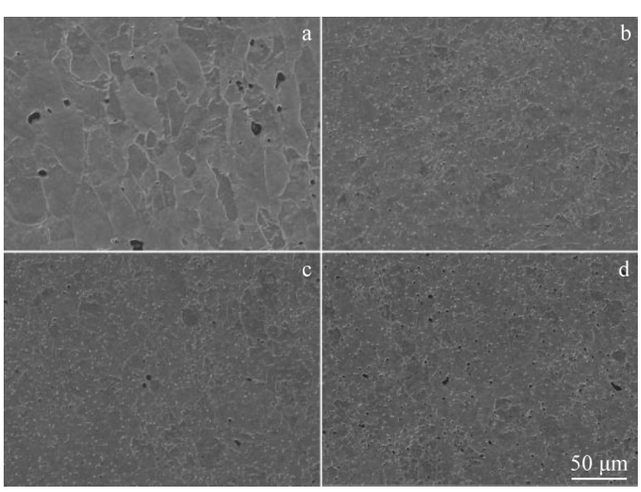


Fig. 2 SEM images of TZM alloys with different $ZrO_2$ contents: (a) pure TZM; (b) 0.5wt%; (c) 1.0wt%; (d) 1.5wt%

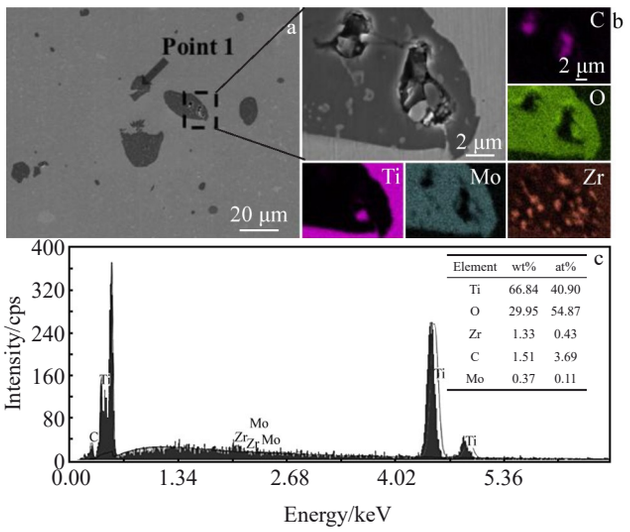


Fig.3 Microstructure (a), EDS element mappings (b), and EDS point scanning results (c) on the surface of pure TZM alloy

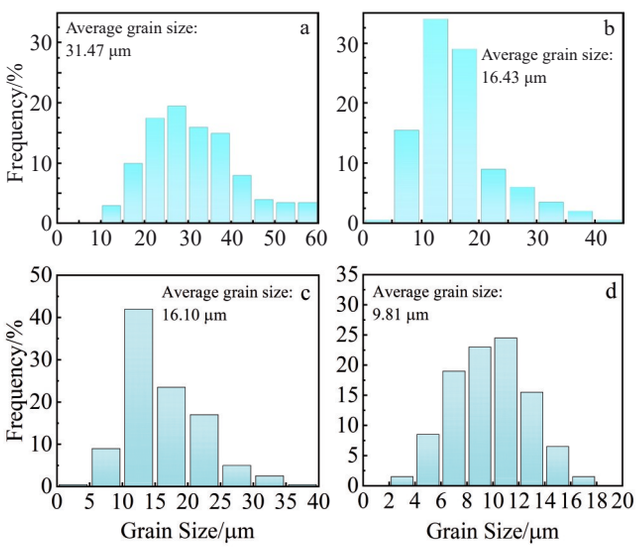


Fig.4 Particle size of TZM alloys with different contents of $ZrO_2$: (a) pure TZM; (b) 0.5wt%; (c) 1.0wt%; (d) 1.5wt%

the second-phase particles are spherical, with a radius of $R$ and a volume fraction of $\theta$, the recrystallized grain size $D$ can be expressed by Eq.(1)[26–27]:

$$D=4R/3\theta \quad (1)$$

The SEM image and EDS mappings of TZM alloy with 1.5wt% $ZrO_2$ corroded at the grain boundary are given in Fig. 5. Interestingly, it can be seen that $ZrO_2$ is dispersed uniformly in the matrix in two forms. One is the larger ellipse located at the grain boundary, as shown by the green arrows in Fig.5, and the other is a smaller regular circle in the crystal, as shown by the red arrows in Fig. 5. These two forms of $ZrO_2$ distributed in TZM alloy can synergistically strengthen the matrix and produce a large number of grain boundaries and phase boundaries. The strengthening mode of intragranular $ZrO_2$ is dislocation strengthening, which improves the strength of the alloy, while the effect of intergranular $ZrO_2$ on dislocation slip is small, and the strengthening mode is fine grain strengthening. Fig. 6 superimposes the grain boundary diagram and phase distribution diagram of TZM alloys with different $ZrO_2$ contents. Red represents molybdenum matrix and green represents zirconia particles. The $ZrO_2$ particles are mainly distributed at the grain boundary junctions, further verifying that the $ZrO_2$ particles hinder the migration of the boundary and are the main reason for the grain refinement. To understand the effect of $ZrO_2$ on the grain morphology of TZM alloy more clearly, EBSD was used to characterize the alloy. Fig. 7 shows the inverse pole figures (IPFs) of TZM alloy. The alternation of red and green color indicates that there are mainly two grain orientations of [001] and [101]. With the addition of the second-phase $ZrO_2$ particles, the proportion of [101] orientation is increased, and [101] is the preferred orientation.

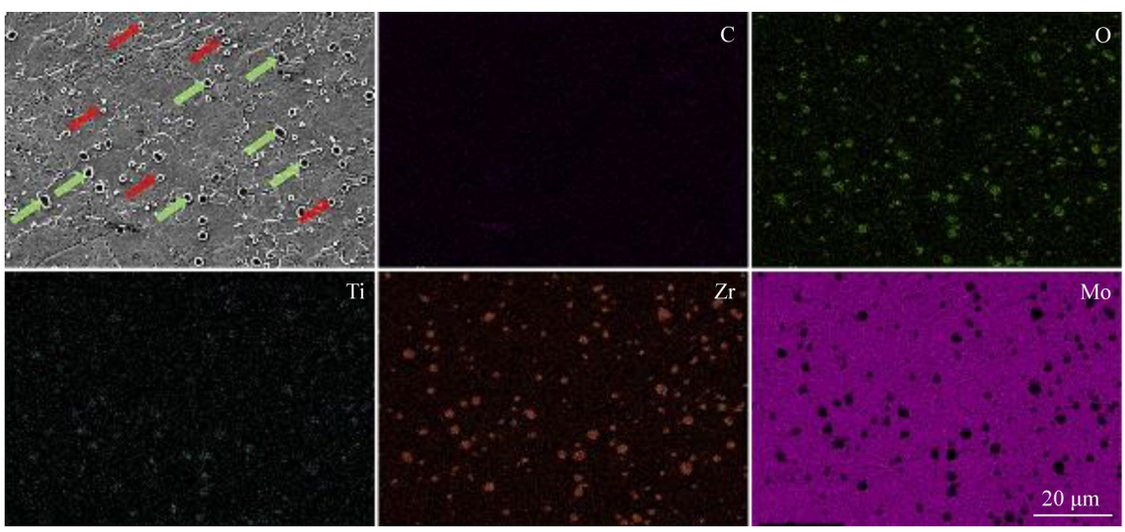


Fig.5 SEM image and corresponding EDS element mappings of TZM alloy added with 1.5wt% $ZrO_2$

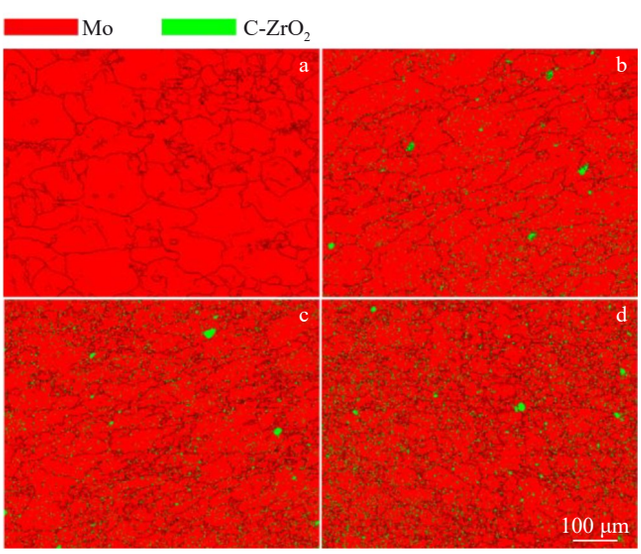


Fig.6 Phase map of TZM alloys with different contents of $ZrO_2$: (a) pure TZM; (b) 0.5wt%; (c) 1.0wt%; (d) 1.5wt%

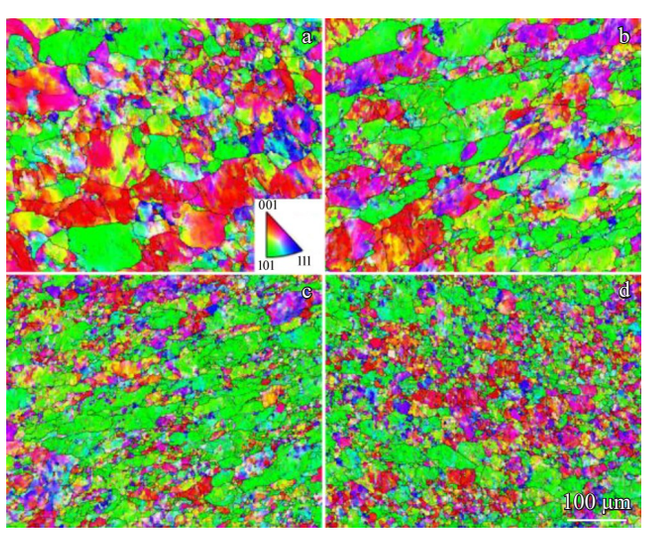


Fig.7 IPFs of TZM alloys with different contents of $ZrO_2$: (a) pure TZM; (b) 0.5wt%; (c) 1.0wt%; (d) 1.5wt%

In general, the alloying elements Ti and Zr in TZM alloys not only play a role in solid solution strengthening, but also form a small amount of strengthening phases TiC and ZrC, which are dispersed with C[4,28–29]. XRD patterns of TZM alloys with different $ZrO_2$ contents are given in Fig. 8. It can be seen that $MoO_2$ is formed with the matrix Mo, due to the similar crystal structure of atoms Mo and Ti, which can form Ti-Mo solid solution that is easily oxidized[17]. The reason why $ZrO_2$, TiC, and ZrC are not observed may be that the content of Ti and Zr is very low, and is less than the detection threshold of XRD.

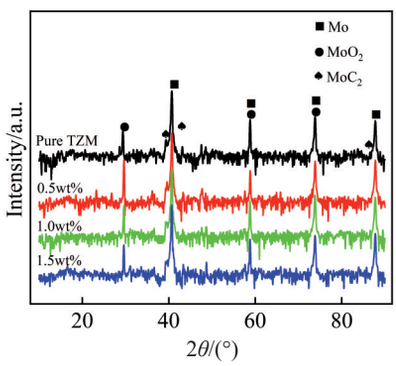


Fig.8 XRD patterns of TZM alloys with different contents of $ZrO_2$

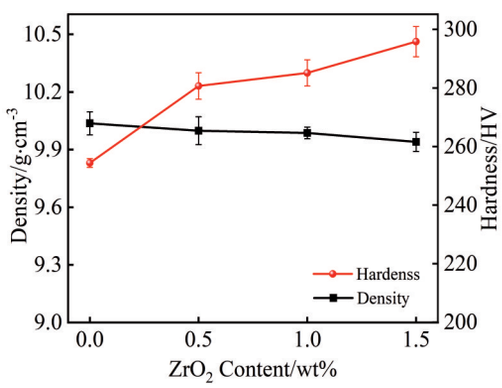


Fig.9 Hardness and density changes of TZM alloys with different contents of $ZrO_2$

### 3.2 Density and hardness of TZM alloy

Fig. 9 shows the hardness and density changes of TZM alloys with different contents of $ZrO_2$. The hardness of TZM alloy increases with the increase in $ZrO_2$ content, and reaches the maximum of 295 HV at 1.5wt% $ZrO_2$, which is about 16.7% higher than that of pure TZM, due to grain refinement[30]. The density decreases with the increase in $ZrO_2$ content. The density of pure TZM alloy is 10.037 g/cm$^3$, and the density of TZM alloy added with 1.5wt% $ZrO_2$ is the lowest (9.968 g/cm$^3$). The reduction in density can be attributed to the fact that the density of $ZrO_2$ (5.6 g/cm$^3$) is considerably lower than that of TZM (10.088 g/cm$^3$).

### 3.3 Abrasive wear performance

Fig. 10 shows the mass loss of the tested materials worn by different sandpapers, including 400, 800, 1200, and 1500 CW, corresponding to abrasive particle sizes of 38, 18, 11, and 7 μm, respectively, under different load conditions. The mass loss increases with the increase in abrasive grain size and load, and the mass loss of samples added with 1.5wt% $ZrO_2$ is the lowest under all loads with the same abrasive particle size. Fig. 11 is an isoline diagram of the interaction between abrasive particle size and load. It can be seen that when the particle size and load reach the maximum, the abrasive wear of the alloy is more serious, but TZM alloy with 1.5wt% $ZrO_2$ has the least red zone and better abrasive wear resistance, which is consistent with the analysis of the wear amount of TZM alloy.

Fig. 12 illustrates abrasive wear morphologies of the sample worn under 20 N by sandpaper 1200 CW (11 μm). The wear mode of samples is mainly micro-cutting and micro-ploughing, and the main characteristics of the worn surface are cutting furrows with different depths and numbers. In Fig. 12a, there are more and deeper grooves on the wear surface of pure TZM alloy, which is due to the deeper penetration of abrasive particles into the matrix, resulting in increased wear. In Fig. 12b – 12d, with the increase in $ZrO_2$ content, the wear surface is obviously improved. The wear surface of TZM alloy containing 1.5wt% $ZrO_2$ is relatively smooth, with few grooves and shallow depth, which effectively protect the matrix. In Fig. 12d, it can be observed that when the groove passes through the oxide, the groove

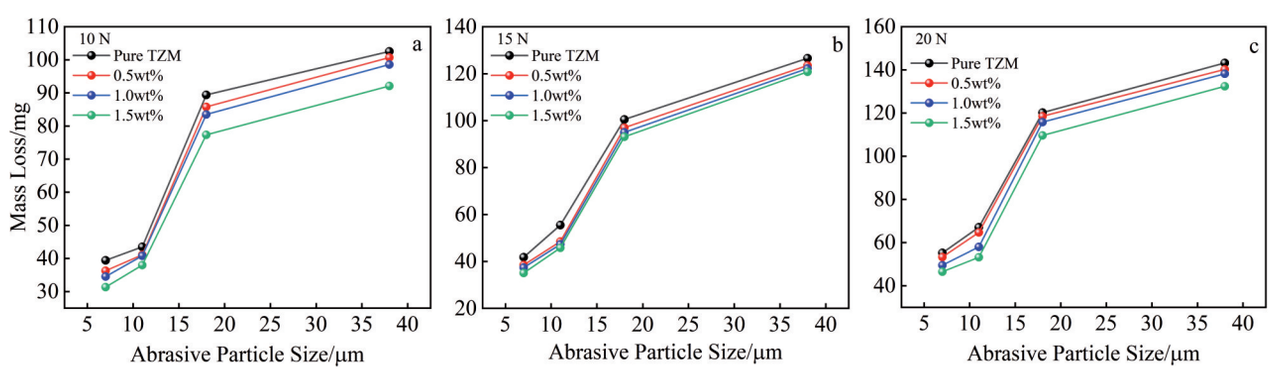


Fig.10 Mass loss of TZM alloys under different loads and abrasives: (a)10 N; (b)15 N; (c) 20 N

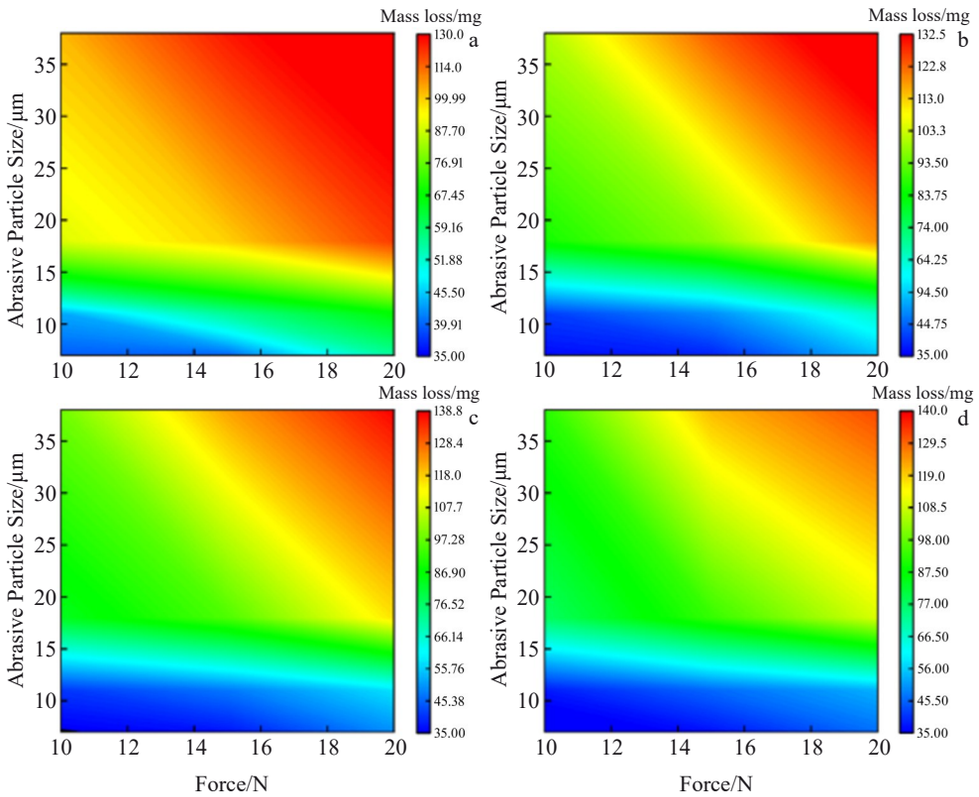


Fig.11 Effect of abrasive and load on wear performance of TZM alloys: (a) pure TZM; (b) 0.5wt%; (c) 1.0wt%; (d) 1.5wt%

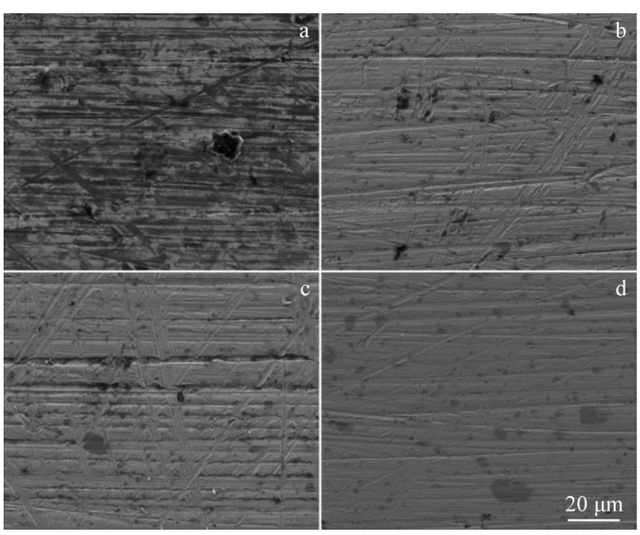


Fig.12 Abrasive wear morphologies of materials at 20 N and abrasive particle size of 11 μm: (a) pure TZM; (b) 0.5wt%; (c) 1.0wt%; (d) 1.5wt%

becomes shallower and thinner, and the oxide prevents the abrasive particles from penetrating into the matrix, thus leading to a deeper groove. Fig. 13 shows the EDS results of the worn surface of TZM alloy containing 1.5wt% $ZrO_2$ (Fig. 12d), showing that most of the dark areas are $ZrO_2$ particles. The second-phase $ZrO_2$ in the alloy plays a certain reinforcing role. On the one hand, it blocks the abrasive particles. On the other hand, the addition of the second-phase particles refines the grains of the matrix and improves its overall strength and hardness.

Fig. 14 illustrates three-dimensional (3D) morphologies of the test materials at different abrasive particle sizes under the load of 20 N. When the abrasive particles are small, the wear surface of the material is relatively smooth, and only some shallow and thin grooves appear. With the increase in abrasive particle size, the wear degree of surface is gradually aggravated, the grooves become deeper and wider, and the number is also obviously increased. At the same abrasive particle size, with the increase in $ZrO_2$ content, the wear surface gradually flattens. For verification, as show in Fig. 15, the two-dimensional (2D) depth contour line measured in the middle area of each sample in Fig. 14 shows that the contour line of TZM alloy with 1.5wt% $ZrO_2$ is smoother and shallower at all abrasive particle sizes, because the hardness and toughness of $ZrO_2$ are higher, and it is not easy to be ground by abrasive particles, which hinders the depth of the penetration of abrasive particles into the matrix Mo, and thus a lot of mass loss and furrows will not occur on the wear surface. This is because at the initial stage of wear, $ZrO_2$ and the matrix are at the same level, and both contact with the abrasive at the same time under the action of load, which will produce cutting and plastic deformation in the matrix. With continuous wear, the matrix is sunken, the abrasive flattens the plastic deformation zone of the matrix, the scratches become smooth, and the second-phase $ZrO_2$ particles protrude from the surface of the machine body. At this time, when the alloy surface is worn, the abrasive contacts with the $ZrO_2$ firstly, so

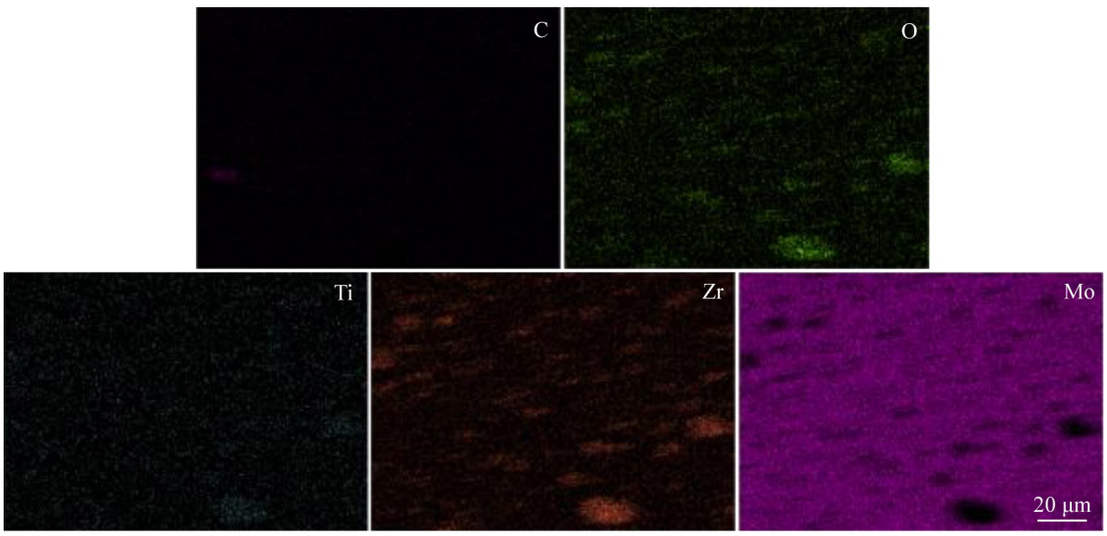


Fig.13 EDS element mappings of TZM alloy containing 1.5wt% $ZrO_2$ shown in Fig.12d

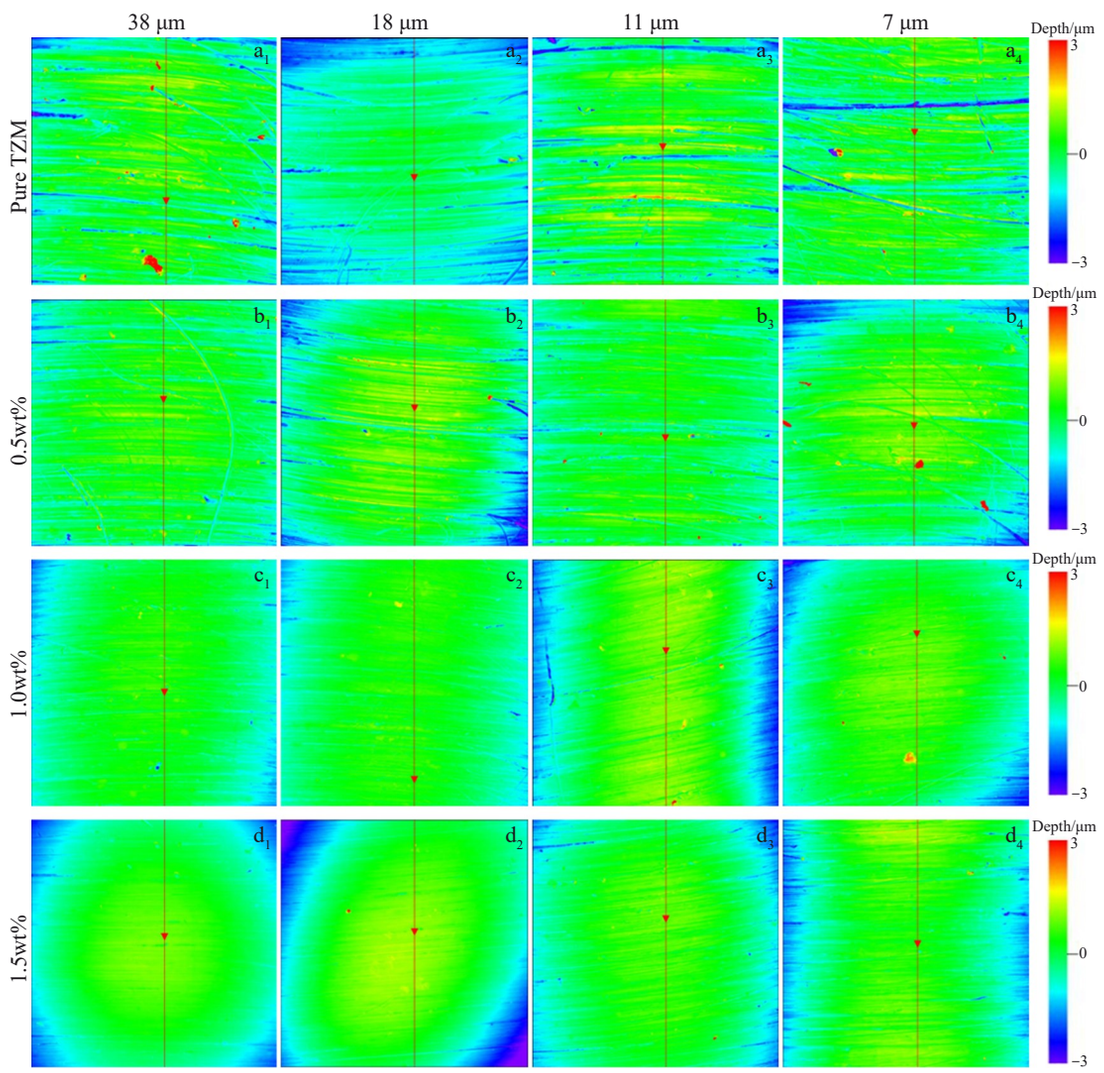


Fig.14 3D-topography morphologies of TZM alloy with different contents of $ZrO_2$ at different abrasive particle sizes under the load of 20 N

that the possibility of contact between the sunken matrix and the abrasive is reduced, the matrix is protected, and the wear amount is reduced. With the prolongation of wear time, some $ZrO_2$ which is not closely combined with the matrix is cut off

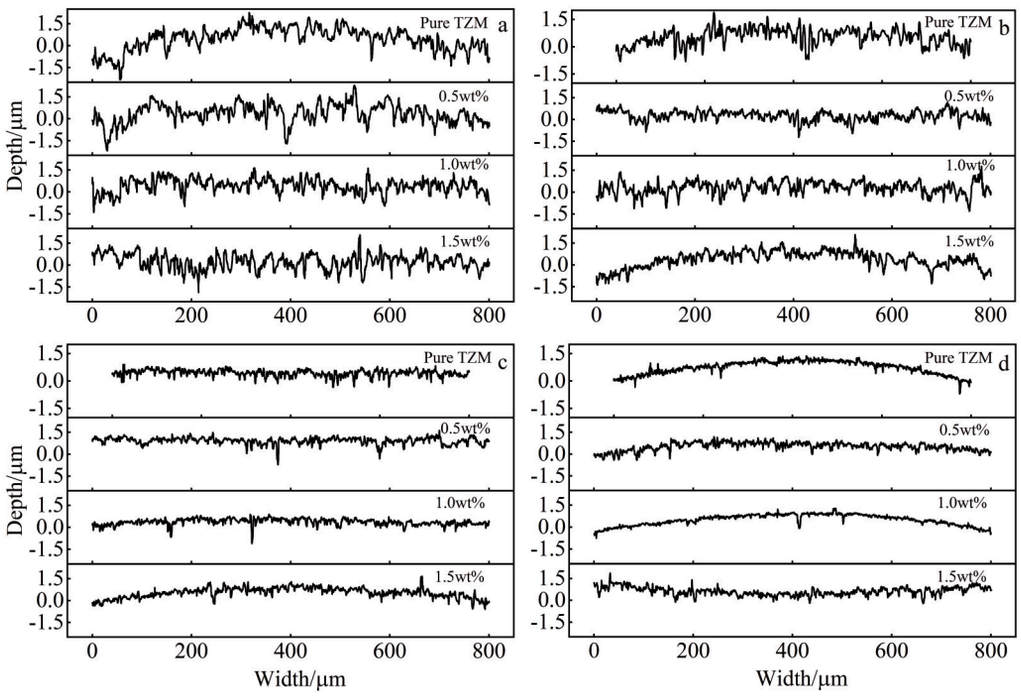


Fig.15 2D depth contour line profiles of worn surface of TZM alloy with different contents of $ZrO_2$ at different abrasive particle sizes: (a) 38 μm; (b) 18 μm; (c) 11 μm; (d) 7 μm

or peeling off due to repeated contact with abrasive particles, resulting in fatigue wear, and thus pits appear.

### 3.4 Reason for excellent wear resistance of TZM alloy added with $ZrO_2$

The main form of abrasive wear is micro-cutting. In the wear process, in addition to two-body abrasive wear, there are also three-body abrasive wear. In this case, abrasive particles and second-phase particles fall off the friction pair and TZM alloy, and furrows with different depths will form on the worn surface. There are three main reasons why TZM alloy with 0.5wt% $ZrO_2$ has excellent abrasive wear performance. Firstly, the added high-hardness $ZrO_2$ is evenly distributed on the alloy surface, which improves the hardness of TZM alloy and can effectively resist abrasive scratches. Secondly, the distribution of $ZrO_2$ at the grain boundary prevents grain boundary migration and refines grains to strengthen the matrix, which plays an important role in improving the strength of materials. Thirdly, with the continuous loss of matrix during the wear process, $ZrO_2$ is exposed to become the main bearer of load to resist the cutting of abrasive particles, so the worn surface of the alloy is not easily broken by hard abrasive particles even under the action of high stress, which is beneficial to improve its wear resistance.

## 4 Conclusions

1) According to the grain size distribution, the grain size of TZM alloy decreases with the increase in $ZrO_2$ content, and it is significantly refined from 31.47 μm to 9.81 μm, which is mainly due to $ZrO_2$ distribution at grain boundaries, which hinders the migration of grain boundaries and thus refines the alloy grains.

2) The hardness of TZM alloy with 1.5wt% $ZrO_2$ reaches a maximum of 295 HV, which is about 16.7% higher than that of pure TZM, due to grain refinement.

3) The wear loss of the alloy increases with increasing load and abrasive grit size, and decreases with increasing $ZrO_2$ content. The wear loss of TZM alloy with 1.5wt% $ZrO_2$ is the least. Therefore, the wear resistance of TZM alloy is improved by adding $ZrO_2$. This is attributed to the combination of high-hardness $ZrO_2$, $Mo_2C$, and oxides, which effectively resist the damage of abrasive.

4) During the wear process, the wear mechanism is mainly micro-cutting, and the wear morphology of the alloy changes under different wear conditions, mainly in terms of the depth and number of furrows. Through the 3D morphology analysis, it can be concluded that the wear surface of TZM alloy with 1.5wt% $ZrO_2$ is relatively flat and smooth under the same wear condition.

## References

1 Meng X C, Li L, Li C L *et al. Corrosion Science*[J], 2022, 200: 110202

2 Xuan C N, Zhu D H, Li C J *et al. Nuclear Materials and Energy*[J], 2023, 34: 101377

3 Danisman C B, Yavas B, Yucel O *et al. Journal of Alloys and Compounds*[J], 2016, 685: 860

4 Tuzemen C, Yavas B, Akin I *et al. Journal of Alloys and Compounds*[J], 2019, 781: 433

5 Peng Zhen, Guo Qingyu, Sun Jian *et al. Rare Metal Materials*

*and Engineering*[J], 2024, 53(1): 17
6 Hu P, Zuo Y G, Li S L *et al. Journal of Alloys and Compounds*[J], 2021, 870: 159429
7 Siller M, Lang D, Schatte J *et al. International Journal of Refractory Metals and Hard Materials*[J], 2018, 73: 199
8 Chakraborty S P, Banerjee S, Sharma I G *et al. Journal of Alloys and Compounds*[J], 2009, 477(1–2): 256
9 Hu Ping, Song Rui, Wang Kuaishe *et al. Rare Metal Materials and Engineering*[J], 2017, 46(5): 1225
10 Hu Ping, Yu Zhitao. *Rare Metal Materials and Engineering*[J], 2017, 46(12): 3961
11 Zhang Z, Li X, Almandoz E *et al. Tribology International*[J], 2017, 110: 348
12 Jing K, Liu R, Xie Z M *et al. Acta Materialia*[J], 2022, 227: 117725
13 Hu P, Yang F, Deng J *et al. Journal of Alloys and Compounds*[J], 2017, 711: 64
14 Xu L, Wei S Z, Zhang D D *et al. International Journal of Refractory Metals and Hard Materials*[J], 2013, 41: 483
15 Cui C P, Zhu X W, Liu S L *et al. Journal of Alloys and Compounds*[J], 2018, 768: 81
16 Zhou H, Zhang Y P, Hua X H *et al. Wear*[J], 2014, 319(1–2):184
17 Sirali H, Şimşek D, Özyürek D. *Metals and Materials International*[J], 2020, 27(10): 4110
18 Sirali H, Simsek D, Ozyurek D. *Transactions of the Indian Institute of Metals*[J], 2022, 75(3): 805
19 Xu Z N, Jiao Z L, Wei S Z *et al. International Journal of Refractory Metals and Hard Materials*[J], 2023, 113: 106183
20 Cui C P, Gao Y M, Wei S Z *et al. Applied Physics A*[J], 2016, 122(3): 214
21 Li S L, Hu P, Liu T *et al. International Journal of Refractory Metals and Hard Materials*[J], 2023, 112: 106152
22 Li S L, Hu P, Han J Y *et al. Materials Characterization*[J], 2022, 186: 1118000
23 Hu B L, Wang K S, Hu P *et al. Journal of Alloys and Compounds*[J], 2018, 757: 340
24 Li S L, Hu P, Zuo Y G *et al. International Journal of Refractory Metals and Hard Materials*[J], 2022, 103: 105768
25 Li Z, Xu L J, Wei S Z *et al. Journal of Alloys and Compounds*[J], 2018, 769: 694
26 Chen L, Wang J S, Zhou F *et al. Journal of Alloys and Compounds*[J], 2018, 735: 2685
27 Olgaard D L, Evans B. *Journal of the American Ceramic Society*[J], 2005, 69(11): 272
28 Wesemann I, Hoffmann A, Mrotzek T *et al. International Journal of Refractory Metals and Hard Materials*[J], 2010, 28(6): 709
29 Ahmadi E, Malekzadeh M, Sadrnezhaad S K. *International Journal of Refractory Metals and Hard Materials*[J], 2011, 29(1): 141
30 Cui C P, Zhu X W, Liu S L *et al. Journal of Alloys and Compounds*[J], 2018, 752: 308

# 氧化锆含量对TZM合金显微组织和磨粒磨损性能的影响

杨亚杰[1]，徐流杰[1,2]，方　宏[3]，李　洲[2]，李秀清[2]，魏世忠[2]
(1. 河南科技大学 材料科学与工程学院，河南 洛阳 471000)
(2. 河南科技大学 金属材料磨损控制与成型国家联合工程研究中心，河南 洛阳 471003)
(3. 丰联科光电(洛阳)有限公司，河南 洛阳 471000)

**摘　要：**采用粉末冶金和轧制法制备了不同$ZrO_2$含量的TZM合金，研究了TZM合金的晶粒尺寸、硬度和耐磨粒磨损性能。对TZM合金在10、15、20 N和磨料粒径为7、11、18、38 μm的条件下进行磨粒磨损试验。结果表明，TZM合金中添加的$ZrO_2$颗粒主要分布在晶界处。含1.5wt% $ZrO_2$的TZM合金晶粒显著细化，硬度提高了16%。磨损试验结果表明，含1.5wt% $ZrO_2$的TZM合金在所有载荷和磨粒尺寸下具有最低的失重率和优异的耐磨性能，磨损性能最高提高了12%。高硬度的$ZrO_2$成为载荷的主要承担者，并且作为第二相阻碍磨粒刺入基体，有效地抵抗磨粒划伤，是优异耐磨性的主要原因。

**关键词：**TZM合金；氧化锆；磨粒磨损；晶粒尺寸

作者简介：杨亚杰，男，1999年生，硕士生，河南科技大学材料科学与工程学院，河南 洛阳 471000，E-mail：2456604744@qq.com